In vitro and *in vivo* MR evaluation of internal gradient to assess trabecular bone density

2010 Phys. Med. Biol. 55 5767

(http://iopscience.iop.org/0031-9155/55/19/010)

IOP PUBLISHING PHYSICS IN MEDICINE AND BIOLOGY

Phys. Med. Biol. **55** (2010) 5767–5785 doi:10.1088/0031-9155/55/19/010

In vitro and *in vivo* MR evaluation of internal gradient to assess trabecular bone density

S De Santis[1,2], M Rebuzzi[1,2], G Di Pietro[2], F Fasano[3,4], B Maraviglia[2,4] and S Capuani[1,2]

[1] CNR IPCF UOS Roma, Department of Physics, University of Rome "La Sapienza", Rome, Italy
[2] Department of Physics, University of Rome "La Sapienza", Rome, Italy
[3] Siemens Medical, Milan, Italy
[4] IRCCS Santa Lucia Foundation, Rome, Italy

E-mail: silvia.capuani@roma1.infn.it

Received 19 February 2010, in final form 17 August 2010
Published 16 September 2010
Online at stacks.iop.org/PMB/55/5767

Abstract

Here we propose a new magnetic resonance (MR) strategy based on the evaluation of internal gradient (G_i) to assess the trabecular bone (TB) density in spongy bone. Spongy bone is a porous system characterized by a solid trabecular network immersed in bone marrow and characterized by a different relative percentage of water and fats. Using a 9.4 T MR micro-imaging system, we first evaluated the relative water and fat G_i as extracted from the Spin-Echo decay function *in vitro* of femoral head samples from calves. Indeed, the differential effects of fat and water diffusion result in different types of G_i behavior. Using a clinical MR 3T scanner, we then investigated *in vivo* the calcanei of individuals characterized by different known TB densities. We demonstrate, on these samples, that water is more prevalent in the boundary zone, while fats are rearranged primarily in the central zone of each pore. *In vitro* experiments showed that water G_i magnitude from the samples was directly proportional to their TB density. Similar behavior was also observed in the clinical measures. Conversely, fat G_i did not provide any information on spongy-bone density. Our results suggest that water G_i may be a reliable marker to assess the status of spongy bone.

1. Introduction

Bone tissue is a complex biomaterial composed of a solid mineral matrix filled by bone marrow (the liquid interstitial phase). The solid matrix is composed mainly of mineral components, while bone marrow is composed mainly of hematopoietic marrow and fatty acid triglycerides at different relative percentages. The relative concentration of each bone marrow component is dependent on both, its anatomical skeletal location and the age of the individual (Liney *et al*

2007). Mammalian and human bone may be classified as cortical or trabecular. The former is mainly present in the shaft of long bones and is much denser (with a porosity ranging from 5% to 10%) than trabecular bone (TB). Conversely, TB, or spongy bone, is much more porous (with a porosity ranging from 50% to 90%) and is metabolically more active. From a physical point of view, spongy bone is a porous system that can be described as a solid with holes and cavities (i.e. presenting as connected void spaces randomly distributed within a solid matrix).

Osteoporosis is a highly diffuse disease that typically affects elderly individuals. It is a systemic skeletal disease characterized by low bone density, micro-architectural deterioration of the bone tissue and by an increase in bone porosity (Bousson *et al* 2000, 2004), leading to bone fragility and increased susceptibility to fracture (WHO Scientific Group Report 2000). From an epidemiological viewpoint, in elderly individuals the occurrence of bone fractures mainly affects those skeletal locations which are particularly rich in TB, such as the vertebrae and femoral head. The evaluation of bone mineral density (BMD) based on dual-energy x-ray absorptiometry (DXA) is currently considered the gold standard for clinical diagnosis of osteoporosis (Kanis and Gluer 2000). However, only a poor correlation between BMD assessments and the relative risk of bone fracture has been reported (Kanis 2002, Wehrli *et al* 2002a), suggesting that other factors besides low BMD likely contribute to determine bone fragility. This lack of information on the risk of bone fracture, which is critical for clinical purposes, has prompted intense research to identify new parameters with the ability to assess spongy-bone status and to provide reliable measures of bone's resistance. A new putative technique has to be first identified theoretically, then tested on *ex vivo* samples, and finally verified *in vivo*, to ascertain its potential utility for clinical purposes. Magnetic resonance (MR) is a non-invasive technique which is able to provide information on the relaxation and diffusion properties of water and fat protons from soft biological tissues such as bone marrow. Therefore, when applied to the investigation of spongy bone, MR provides information on bone marrow which is strictly linked to the surrounding trabecular architecture of the bone due to the mutual interaction between the solid matrix and liquid phase (Wehrli *et al* 2006). In this context, the apparent transverse relaxation time T_2^* was the first MR parameter to be considered as a new surrogate marker for osteoporosis. Indeed, T_2^* probes the micro-structure of TB due to its sensitivity to the microscopic field in-homogeneities caused by magnetic susceptibility differences between the solid bone structure and the liquid bone marrow (Majumdar *et al* 1991, Chung *et al* 1993). Several studies have consistently reported that an increase in inter-trabecular space, which typically occurs in patients with osteoporosis, prolongs the corresponding T_2^* values (Wehrli *et al* 1991, 2002a, Link *et al* 1998). However, the large standard deviation (SD) associated with average T_2^* values assessed in bone tissue from healthy, osteopenic and osteoporotic individuals does not allow the clinical use of T_2^* on a single subject basis (Capuani *et al* 2008).

In this paper we propose an alternative way to quantify the influence of susceptibility changes in spongy bone based on a new MR parameter (the internal gradient G_i that we demonstrate to be strictly associated with TB density and structural rearrangements). Estimation of G_i can be obtained by extraction of this parameter from the Spin-Echo (SE) decay, which is traditionally used for the investigation of porous systems (Watson and Chang 1997, Wilson and Hurlimann 2006, Kuntz *et al* 2008). In a SE sequence, signal refocusing is obtained by reversing the de-coherence effects of spins caused by the distribution of local fields. This method is valid only when molecular diffusion is not taken into account. Diffusion of liquid state protons in local magnetic field gradients (internal gradients G_i) results in a more than expected rapid loss of coherence from the usual spin–spin interaction and surface effects (Watson and Chang 1997, Capuani *et al* 2005). In SE measurements, the additional decay of the echo amplitude is due to the diffusion of fluid molecules in the local magnetic field gradient

G_i generated by the difference in magnetic susceptibility between bone marrow and solid bone plates. As a consequence, in systems like spongy bone, it is possible to assess the intensity of G_i from the attenuation of SE decay. In spongy bone, G_i values are not only affected by differences in magnetic susceptibility between bone marrow and solid bone plates, but also between fat and water diffusion in TB marrow. Moreover, G_i depends on the orientation of the trabecular plates with respect to the external magnetic field (Chung *et al* 1993, Hwang and Wehrli 1995). Some previous works have focused on these G_i features in order to assess the preferential orientation of trabeculae due to loading optimization (Chung *et al* 1993, Mertens *et al* 2008). Recently, a new MR approach based on the detection of spin diffusion through an internal magnetic field gradient has been proposed to characterize TB (Sigmund *et al* 2008, 2009). This approach is based on measuring the G_i to encode diffusion weighting to extract structural information (e.g., surface-to-volume ratio of spongy-bone pores) from the resulting signal decay.

In all these situations, G_i seems to be a potential surrogate marker reflecting different structural features of TB. They include not only the solid phase density, but also other characteristics related to spongy-bone quality (as expressed by water/fat concentrations within the bone marrow).

The aim of the present work was to assess the potential ability of G_i to describe spongy-bone status as related to its TB density and quality. For this purpose, using a micro-imaging probe we investigated *in vitro* at high magnetic field (9.4 T) G_i behavior inside each single pore of calf spongy-bone samples (extracted from a femur head) as a function of both TB density and relative fat and water–bone marrow concentrations. To test the methodological feasibility of this approach, we first quantified mean G_i in calf samples characterized by different TB densities. We then, investigated the potential suitability of G_i as a measure able to assess the TB status *in vivo*. For this purpose, using a 3T clinical scanner, we examined the calcanei of subjects with different TB densities.

2. Theory and methods

2.1. Theory

The signal decay of a SE sequence is usually described by the following equation (Hahn 1950):

$$S(TE) = S_0 \exp\left[-\frac{TE}{T_2}\right], \tag{1}$$

where S_0 is the signal intensity at $TE = 0$, TE is the echo time and T_2 is the transverse spin–spin relaxation time. However, in systems which are strongly influenced by the presence of internal magnetic field gradients G_i, the SE decay is no longer described as a simple exponential decay. In the linear gradient approximation, the signal decay can indeed be expressed by the following equation (Carr and Purcell 1954, Majumdar and Gore 1988):

$$S(TE) = S_0 \exp\left[-\frac{TE}{T_2^{\text{true}}} - \frac{(\gamma G_i)^2 D(TE)^3}{12}\right], \tag{2}$$

where γ is the gyromagnetic ratio, D is the diffusion coefficient and $T_2{}^{\text{true}}$ is the spin–spin relaxation time in which the effects of diffusion and field inhomogeneities are averaged out.

In systems like spongy bone, it is possible to assess the intensity of mean G_i from the attenuation of the SE signal as a function of different TEs. Furthermore, a measure of the diffusion coefficient D (i.e. a measure of the apparent diffusion coefficient (ADC)) and/or a measure of $T_2{}^{\text{true}}$ are needed to reduce the number of unknown parameters and improve the fit

quality. In all *in vitro* and *in vivo* experiments reported in this paper, the ADC was measured and inserted in equation (2) to extract G_i and T_2^{true} using a fitting procedure.

2.2. *In vitro experiments*

Experiments were performed using a Bruker Avance-400 high-resolution spectrometer operating at 9.4 T with a micro-imaging probe (10 mm internal diameter), equipped with a gradient unit characterized by a maximum gradient strength of 1200 mT m^{-1} and a rise time of 100 μs. XWINNMR® and ParaVision® 3.0 software were employed for data acquisition and analysis.

Five *ex vivo* spongy-bone samples, excised from calf femur head, were cut into pieces of approximately 20 mm high and 7 mm deep in order to fit into the micro-imaging probe bore. The long axis of each sample was located parallel to the main direction of the static magnetic field (the z-axis). The temperature of each sample was fixed to 291 K. T_2^*-weighted (Gradient Echo, GE) and T_2-weighted (SE) images were obtained for initial evaluation of TB density. All samples were characterized by a non-uniform trabecular density. As shown in figure 1, TB density varies continuously along the height of each sample, moving from the upper to the lower zone. The upper zone, which is close to the cortical bone, is characterized by higher trabecular density and smaller spongy-bone pores (figure 1(a)). Conversely, the lower zone is characterized by a larger inter-trabecular space (figure 1(c)). The middle zone (located between upper and lower zones) shows intermediate characteristics of TB density (figure 1(b)). Throughout the paper, we will refer to these three anatomical locations as follows: (a) HTD (high trabecular density; upper zone), (b) ITD (intermediate trabecular density; middle zone) and (c) LTD (lower trabecular density; lower zone). In each sample, for each considered location, we identified three 0.2 mm thickness slices to measure quantitative MR parameters. Data extracted from each of the three slices were then averaged to obtain mean values of each MR parameter in the three locations (HTD, ITD and LTD). Five analyzed samples were selected such that they were characterized by similar TB densities and similar fat-to-water ratio quantities in bone marrow. TB density and bone marrow water content (together with the relative content of different types of fat in bone marrow) are known to be dependent on age, race and skeletal site. To correct for these potential biases, we obtained all our samples from 10- to 12-month-old calves of German race, bred in Germany and butchered in Rome (Italy). In all fresh samples (analyzed immediately after slaughter) we identified the same area of the femur head for MR investigation.

2.2.1. Spectroscopic experiments. In the first step of our experiments, a validation experiment was performed under ideal circumstances where molecular diffusion and T_2 information were obtained for each of the two individual spectral components (water and fat molecules).

A spectroscopic Carr–Purcell–Meiboom–Gill (CPMG, repetition time $TR = 1$ s, number of averaged scans $NS = 8$, $N = 64$ data points, (corresponding to 64 echoes refocusing every 2 ms from 1 to 127 ms) and a spectroscopic pulsed field gradient stimulated echo (PGSE, $TE/TR = 18/3000$ ms, diffusion gradient pulses delay $\Delta = 400$ ms, diffusion gradient pulses duration $\delta = 4.6$ ms and diffusion gradient strength g applied along the x-axis using 32 gradient amplitude steps from 6 to 100 mT m^{-1}) were used to recognize and discriminate T_2 and ADC of water and fat molecules in the samples.

2.2.2. Spatially resolved experiments. A MSME (multi-slice multi-echo) imaging sequence ($TR = 2000$ ms, field of view FOV = 7 mm, matrix 256 × 256, slice thickness, STH = 0.2 mm, pixel dimensions 27 × 27 μm^2, $NS = 8$) at various TEs (4.8, 6, 8, 10, 12, 14, 16, 18, 20, 24,

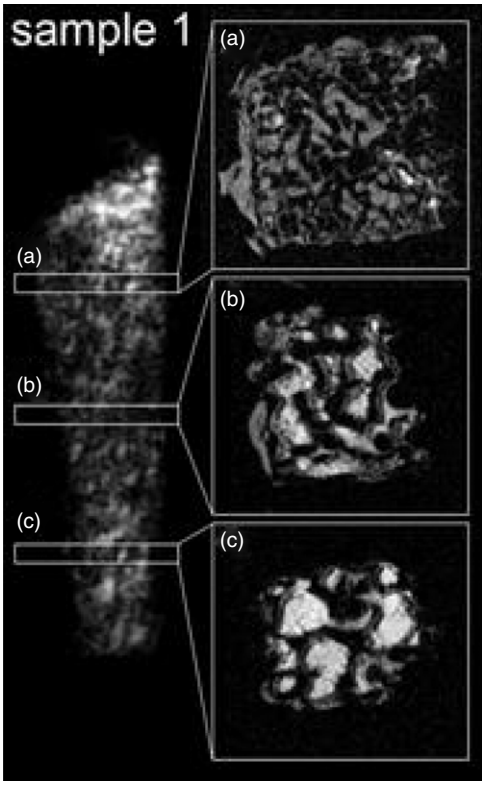

Figure 1. An example of the calf spongy-bone sample used for experiments *in vitro*. GE localizer and SE images ($TE = 4.3$ ms) selected perpendicularly to the static magnetic field at three different depths in the sample show a non-uniform TB density. In each experimental sample, trabeculae are closely spaced in the upper zone (a). Conversely, they show an intermediate density in the middle zone (b) and a larger inter-trabecular space in the lower zone (c).

30, 40, 50, 60, 70, 80, 100, 120 ms) was used to obtain the SE decay in the three regions of each sample characterized by a different TB density. A PGSTE imaging sequence was also employed ($TE/TR = 21.9/3000$ ms, FOV = 7 mm, matrix 256×256, $\Delta = 40$ ms, $\delta = 4$ ms, using eight b values ranging from 400 to 40 000 s mm^{-2}, STH = 0.2 mm, $NS = 8$) in order to measure the ADC along the x-axis for each of the three selected regions of the considered samples. The b value is related to the aforementioned parameters through the known relation: $b = \gamma^2 g^2(\Delta - \delta/3)$, where g is the diffusion gradient strength. The x-axis was arbitrarily chosen to assess molecular diffusion perpendicular to trabeculae surfaces (see figure 1).

After the micro-imaging investigation of the bone marrow's water and fat behavior within pores of spongy bone, we set up an equivalent acquisition protocol at lower *TE*s (4.8, 10, 20, 40, 60, 80, 100 ms) and b values (ranging from 200 to 10 000 s mm^{-2}). This additional protocol was added to obtain a protocol potentially suitable for clinical application (i.e. lower scan time, lower b values). However, due to a reduced number of experimental points, this acquisition provides SE decays and ADCs that do not clearly discriminate between water and fat.

2.3. Data processing and statistical analysis

T_2 and ADC of water and fat components were obtained using a Levenberg–Marquardt (L–M) fit taking into account the peak area decays respectively centered at 4.7 ppm (large from 4 to 5.4 ppm) for water and at 1.3 ppm (large from 0.1 to 2.5 ppm) for fat. Due to the low resolution of bone marrow spectra in the spongy-bone samples, the olefinic fat peak at 5.3 ppm overlaps the broad water peak centered at 4.7 ppm. For this reason, we fitted the attenuation of this broad peak (from 6 to 4 ppm) versus the diffusion gradient strength or the *TE* value using a bi-exponential function. This took into account the olefinic and water component separately. In figure 2 an example of spectroscopic investigation is shown.

Two different *in vitro* analyzes were performed using the data extracted from the imaging experiments. In both cases we considered only the central zone of each image (i.e. excluding the image border), in order to exclude or limit the presence of air in bone marrow cavities. Indeed, this represents one of the major sources of artifacts when performing imaging on excised samples.

In the first analysis, the signal deriving from water and fat protons in T_2-weighted images was investigated as a function of each voxel location with respect to the bone–bone marrow interface. In each slice of the three considered locations, the signal nearby the boundaries between bone marrow and solid bone was identified using a software (written in Matlab) (figure 3) written in-house.

SE signal properties and G_i behavior were then assessed in the boundary and inner regions of the trabecular pores. The inner regions of the pores were identified by subtracting the boundary regions from the whole pore area. An L–M fit was performed using the signal as a superimposition of two components: one belonging to fats and another belonging to water molecules. Each component contributes to the total signal as one exponential term of formula (2). The signal intensity at $TE = 0$, $T_2{}^{\text{true}}$, G_i and the ADC of water and of fat components were obtained. Using this procedure, mean and SD values of G_i from water and fat were respectively derived. Water ADC and fat ADC were measured from diffusion-weighted images, while $T_2{}^{\text{true}}$ values were considered a free parameter in the fit.

Conventional T_2 relaxation times of water and fat components were also evaluated from the same images, executing a bi-exponential L–M fit of water and fat components, in accordance with formula (1). This analysis was repeated at different widths (measured in voxels) from the boundary region of each pore. The mean values of water and fat G_i were calculated by averaging the results obtained in all pores contained in three image slices for each specific location (HTD, ITD and LTD).

In order to have a more objective quantification of TB density, we calculated the ratio between the perimeter and the area of each pore in the slices. As a result, the ratio (N_p/N_a) between the number of voxels defining each pore perimeter (N_p) and the number of voxels constituting the corresponding area (N_a) was obtained from all pores included in each of the slices. Then, the mean values of N_p/N_a and G_i in different bone locations (characterized by different TB densities as defined by N_p/N_a) were obtained from each sample. Moreover, mean values of both magnetization associated with water and fat extracted from the bi-exponential fit as a function of the boundary region width were evaluated. The averages were calculated in all five samples. Pearson's correlation coefficient (r) and a paired Student's t-test were used to assess the linear correlation between G_i and TB densities and differences between water and fat magnetization as a function of boundary distances measured in voxels.

In a second experiment, G_i was derived using the signal arising from each entire slice. In this case, we aimed to identify an acquisition protocol at high magnetic field which might also be suitable for clinical application (using relatively short acquisition times,

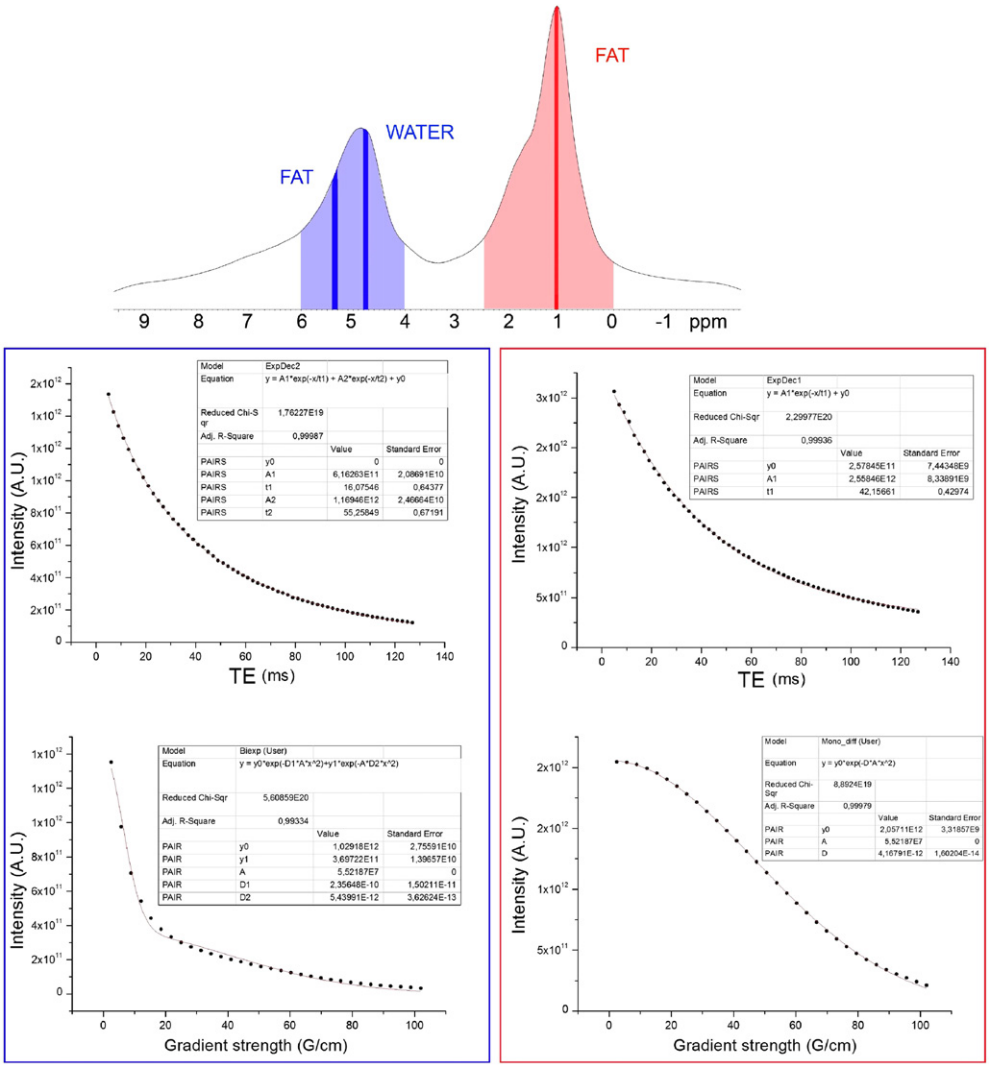

Figure 2. An example of the fitting procedure used in spectroscopic validation experiments to obtain T_2 and ADC of water and fat components. The broad peak on the left side of the spectrum is characterized by two different components: water centered at 4.7 ppm and olefinic fat centered at 5.3 ppm. Peak attenuation versus gradient strength or *TE* value was fitted using a bi-exponential function which took into account olefinic and water components separately. Conversely, the attenuation of fat peak at 1.3 ppm (on the right side of the spectrum) was fitted using monoexponential functions. See the text for further details.

conventional sequences and a lower image resolution compared to that obtained by micro-imaging apparatus). Distinguishing water from fat components was not a priority in this case. Therefore, a monoexponential L–M fit was employed to obtain the mean ADC along the x-axis. A monoexponential L–M fit was performed using formula (2) and included a constant which took into account the deviation from monoexponential behavior. Mean and SD values of G_i were obtained in the three bone locations (HTD, ITD and LTD) performing an average of

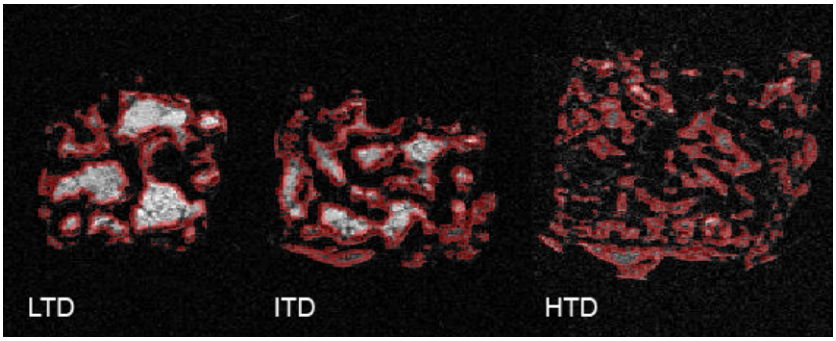

Figure 3. Example of selection of a three pixel wide boundary region in three considered locations, respectively, characterized by lower (LTD), intermediate (ITD), and higher trabecular density (HTD). The red mask, which represents the boundary region, is superimposed over SE images obtained at $TE = 4.3$ ms.

G_i values across the five samples together with their corresponding values of T_2^{true}. Moreover, conventional T_2 relaxation time was estimated from each slice using a monoexponential L–M fit as described by formula (1) plus a constant. Again, mean and SD values of T_2 were obtained in the three zones (HTD, ITD and LTD) by performing an average of T_2 values across the five samples.

2.4. In vivo experiments

Six subjects were recruited for this study, three healthy females (24, 42, 52 years old, respectively), one osteopenic and one osteoporotic female (both subjects 62 years old), and one male (33 years old).

Healthy, osteopenic or osteoporotic status of the 52- and 62-year-old females was established on the basis of their last (within 6 months from our MR investigation) DXA medical report. The mean *T*-score in L1 to L4 vertebrae of the 52- and of the two 62-year-old females were −1.30, −1.81 and −3.51, respectively.

The study was approved by the Local Ethics Committee. Each subject gave her/his informed written consent to participate in this study.

A progressive reduction of TB density across aging has been well described in the previous literature (Wehrli *et al* 1995, Thomsen *et al* 2002). In humans, bone mass reaches a maximum peak at the approximate age of 25 years, and then progressively decreases over the following decades. As a consequence, it is reasonable to assume that both the 42- and the 52-year-old females had a lower TB density when compared to the 24-year-old female. Gender-related differences are also well reported (Mosekilde 2000). Men are known to have a higher bone mass peak than age-matched women, thus suggesting that our male subject had the highest TB density. Moreover, the osteoporotic female (*T*-score = −3.51) included in this study had a lower TB density than the age matched osteopenic (*T*-score = −1.81) female. As expected, both 62-year-old females (with osteopenia and osteoporosis) had a lower TB density than the 52-year-old healthy woman (*T*-score = −1.30).

Each subject underwent an MRI examination of the right foot (figure 4), using a 3T MR system (Siemens Allegra, Erlagen, Germany). A FLASH (Fast Low-Angle SHot) sequence ($TR = 1500$ ms, field of view FOV = 192 mm, matrix 128 × 128, slice thickness 5 mm, flip angle 30°) was acquired using various *TE*s (5, 7, 10, 20 ms) to estimate T_2^*. Sagittal

Figure 4. MR sagittal view of the foot examined in a 24-year-old female. The region outlined in black shows the calcaneal area on the SE image used to assess the mean value of G_i after fitting based on the L–M procedure.

SE images (TR = 1500 ms, FOV = 192 mm, matrix 256 × 256, slice thickness 5 mm) were also collected using a SEMC (spin echo multi contrast) sequence at various TEs (20, 30, 40, 50, 80, 100 ms). The ADC was evaluated from sagittal diffusion-weighted images using a SE segmented-EPI (echo planar image) sequence at two different b values (0 and 8000 s mm^{-2}) with diffusion gradient applied along the anterior–posterior direction and $TE/TR = 89/2500$ ms. G_i was obtained by the same mono-exponential L–M fitting procedure (using equation (2) without discriminating between water and fat components) described in the previous section by selecting the entire calcaneal area of each subject as shown in figure 3. Single voxel spectroscopy (PRESS sequence) with $TE = 22$ ms, $TR = 5$ s, $NS = 32$, was used to obtain bone marrow proton spectra to extract fat and water content percentage. A single voxel (size of 15 × 15 × 15 mm^3) was positioned in the center of the calcaneus of each subject.

3. Results and discussion

3.1. In vitro results

Spectroscopic T_2 and ADC mean values and their SD of water and fat components in excised bone samples are reported in table 1. Data show that both T_2 and ADC of the water component (centered at 4.7 ppm) are significantly lower than those of fat components (centered at 5.3 ppm and 1.3 ppm). This allows us to discriminate clearly between the two components (water and fat). Specifically, T_2 values of water and fat are respectively consistent with those previously reported (Chabanova *et al* 2006). Similarly, ADCs of fat components, which are approximately two order of magnitude lower than those of water molecules, fit well with those recently reported by other authors (Ong *et al* 2009).

In table 2, mean values (and their SD) of T_2, ADC, G_i and T_2^{true} are reported for the water component obtained in LTD, ITD and HTD locations of one sample (performing an average of

Table 1. Spectroscopic evaluation of excised calf samples.

	($T_2 \pm$ SD) (ms)	(ADC $\pm$ SD)	
H_2O at 4.7 ppm	19 ± 7	4.2 ± 1.8	10^{-10} m^2 s^{-1}
Fats at 5.3 ppm	72 ± 36	5.0 ± 0.6	10^{-12} m^2 s^{-1}
Fats at 1.3 ppm	65 ± 16	5.3 ± 0.3	10^{-12} m^2 s^{-1}

Table 2. Results from one excised calf sample: (a) water component and (b) fat component.

			(a) Water component		
	Water (%)	($T_2 \pm$ SD) (ms)	(ADC $\pm$ SD) ($\times 10^{-10}$ m^2 s^{-1})	($G_i \pm$ SD) (mT m^{-1})	($T_2^{\text{true}} \pm$ SD) (ms)
LTD	55	17.0 ± 3.0	19.0 ± 0.4	222 ± 131	17.9 ± 1.0
ITD	47	15.0 ± 2.3	7.0 ± 0.4	282 ± 134	15.2 ± 0.5
HTD	97	14.8 ± 0.4	1.6 ± 0.1	803 ± 181	16.0 ± 0.3
			(b) Fat component		
	Fat (%)	($T_2 \pm$ SD) (ms)	(ADC $\pm$ SD) ($\times 10^{-12}$ m^2 s^{-1})	($G_i \pm$ SD) (mT m^{-1})	($T_2^{\text{true}} \pm$ SD) (ms)
LTD	45	42.3 ± 6.2	5.3 ± 0.3	760 ± 195	43.0 ± 4.8
ITD	53	39.7 ± 4.0	5.9 ± 0.3	727 ± 437	44.0 ± 5.3
HTD	3	31.6 ± 6.0	5.4 ± 0.2	904 ± 119	37.5 ± 9.8

values extracted from each slice belonging to a single location). In table 2, the corresponding results for the fat component are reported.

The water ADC showed a decreasing trend proportional to the increase of trabecular density; thus, water mobility is more restricted in regions where the trabeculae are smaller. Conversely, it is evident from table 2 that the fat ADC is not sensitive to increase in trabecular density. Water G_i increases proportionally with the increase in TB density, while fat G_i is characterized by an opposite trend and does not allow discrimination between LTD and ITD.

Figure 5 displays different types of behavior of water and fat G_i as a function of the distance (in voxels) between the TB marrow interface and the internal part of the trabecular pore. G_i values were derived using a fitting procedure, while ADC values were derived from diffusion-weighted images.

According to our findings, water G_i is characterized by a decreasing trend when moving from zones adjacent to the trabecula to zones located in the center of the inter-trabecular space. This behavior was observed in each of the three locations characterized by different TB densities. When comparing G_i magnitude between the three locations, it was otherwise evident that G_i in the HTD location is higher than that extracted from the other two locations (ITD and LTD). Conversely, fat compared to water G_i revealed an opposite behavior. In the latter case, G_i was characterized by an increasing trend when moving from voxels adjacent to trabeculae to those located in the center of the inter-trabecular space. In the insets of figure 5, mean magnetization intensities are reported for fat and water components as derived from the fitting procedure. Water concentration is higher in the HTD slices and decreases proportionally with the reduction of trabecular density (i.e. in ITD and in LTD).

ADC values and their magnetic susceptibility are the key parameters accounting for the different types of behavior of water and fat G_i (figures 5 and 6). The water ADC is

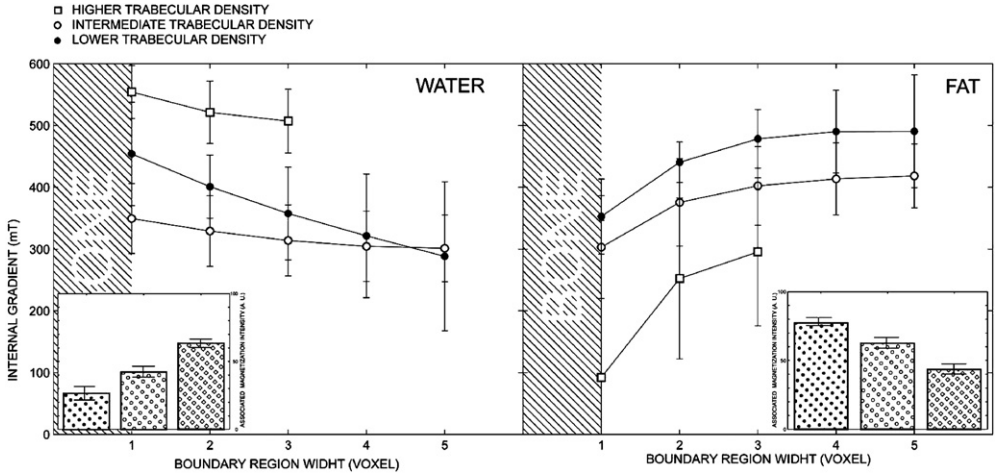

Figure 5. Behavior of water (left) and fat G_i (right) as a function of increasing voxel number ranging from regions with one pixel (located close to the bone surface) to regions constituted by five pixels (from the bone surface to the pore center). Results are reported for HTD (empty squares), ITD (empty circles) and LTD (filled circles). In regions with HTD, the last two points are missing because the trabecular interspaces were not large enough to allow a boundary region (which is wider than three pixels) to be drawn.

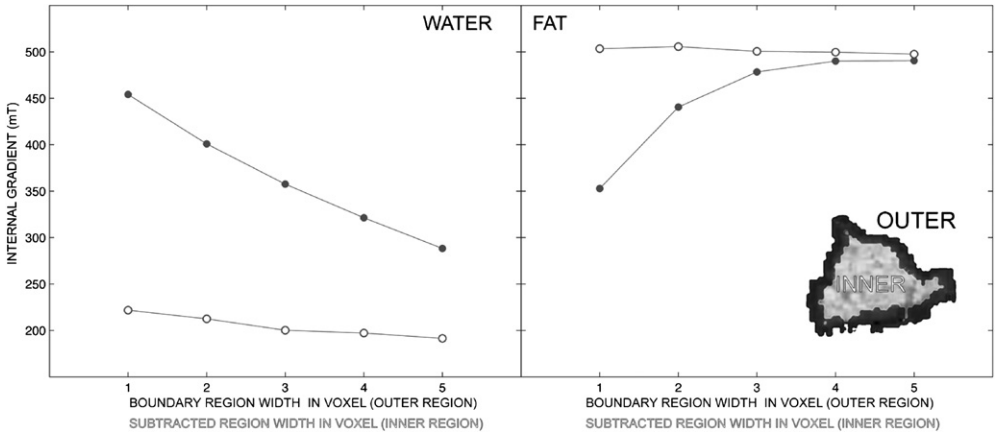

Figure 6. Water G_i (left) and fat G_i (right) behavior for LTD in the boundary region (filled circles) and in the inner region (empty circles) as a function of increasing boundary region width (which corresponds to a decrease of the inner region width). The size of each pixel is 27 μm.

approximately two orders of magnitude higher than the fat ADC. As a consequence, water molecules compared to fat molecules are characterized by a faster motion. According to Einstein's relation $\langle r \rangle^2 = 2Dt$, which links the mean square spatial range spanned by diffusing molecules (characterized by a certain diffusion coefficient D at a diffusion time t), water spins travel a distance of the order of tenths of microns (calculated using the diffusion times Δ employed in this study). Conversely, the displacement of protons in fat lies in the sub-micron range. Moreover, water and fat are characterized by different magnetic susceptibilities:

$\chi_{\text{water}} = -9.05 \times 10^{-6}$ and $\chi_{\text{fat}} = -8.44 \times 10^{-6}$ (SI units) (Szczepaniak *et al* 2002), while bone tissue is believed to be characterized by $\chi_{\text{bone}} = -11 \times 10^{-6}$ (Hwang and Wehrli 1999).

The G_i belonging to protons in water is sensitive to differences in magnetic susceptibility in the range of the pixel dimension. As expected, G_i shows a decreasing trend when moving from the bone–bone marrow interface to the pore center. Indeed, the difference in water–bone susceptibility represents the main source of water G_i. Conversely, protons in fat are sensitive to differences in magnetic susceptibility ranging at least from two orders of magnitude less than the pixel size. For this reason, fat G_i measured in this study cannot be attribuited to the bone–bone marrow interface. Fat G_i magnitude is better explained by the difference in magnetic susceptibility between fat and water. The increasing trend of fat G_i values (when moving from the bone–bone marrow interface to the pore center) can thus be ascribed to a different rearrangement of fat molecules. In the central zone of each pore, there is a higher concentration of fat molecules characterized by a lower molecular motion than that of water molecules. As a consequence, fat G_i in the center of the pore assumes higher values than those observed nearby the bone surface. Indeed, in this latter location, there is a reduced concentration of fat molecules. This means that a correspondingly higher concentration of water molecules (characterized by faster motion) modulates fat G_i by reducing its values. This scenario fits well with the hypothesized distribution of bone marrow filling trabecular pores, for which we could say that 'water wets' the surface of bone pores. On the other hand, fat molecules, due to their hydrophobic nature, are mainly rearranged to lie in the central zone of the pore. As shown in figure 6, water and fat G_i behavior in the boundary and inner regions of LTD pores support this hypothesis. In the figure, water and fat G_i behavior (expressed as a function of increasing pixel width) of the boundary region are compared to those measured from the inner region. G_i values of both water and fat bone marrow components move toward an asymptotic value which is very close to that obtained in the central zone of the trabecular pore.

This observation confirms that water G_i variation is mainly due to bone–bone marrow interface susceptibility properties. Therefore, water G_i might be considered as a surrogate marker of the TB structure. The asymptotic G_i values reached by the fat component were higher when compared to those reached by the water component. Again, the difference in the diffusion coefficient between fat and water might explain these results. As water molecules, compared to fat molecules, are associated with a faster diffusive motion during the experimental diffusion time, water spins are more dependent on motional averaging. As a consequence, the susceptibility dephasing effect which affects the SE signal of water is partially averaged. This peculiar behavior of water/fat systems has already been investigated and verified elsewhere (Lammentausta *et al* 2008). To support the hypothesis that water concentration is higher in the boundary zone of pores, while fat is more concentrated in the central zone of pores, mean magnetization, extracted from the fit and associated with water (left) and fat (right) quantities in the first three voxels of the boundary regions, is reported in figure 7. Mean magnetization values and their corresponding SD values were obtained from all five samples belonging to different calves. Mean magnetization values associated with each voxel's zone of the boundary region are statistically different ($p = 0.05$).

Data reported in figure 7 demonstrate that in each pore of spongy bone, the quantities of water molecules at the bone–bone marrow interface are higher than that of fat molecules. As a consequence, in spongy bone (filled with bone marrow), the measurements of water MR parameters (such as G_i, T_2^* or ADC) best provide information on TB density.

In figure 8 mean G_i values and their SD, obtained from the five samples as a function of their TB density, are reported. The graph in the inset of figure 8 shows a positive linear correlation between water G_i and TB densities (Pearson's correlation coefficient $r = 0.71$).

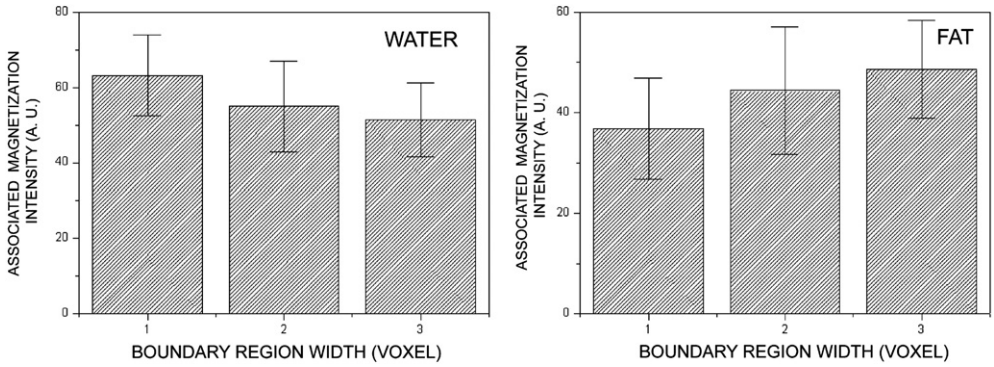

Figure 7. Mean magnetization values arising from the bi-exponential fit associated with water (left) and fat (right) versus boundary region width, expressed as a distance in voxels from the bone/marrow boundary. The average is performed across all samples. LTD location was considered in all experimental samples.

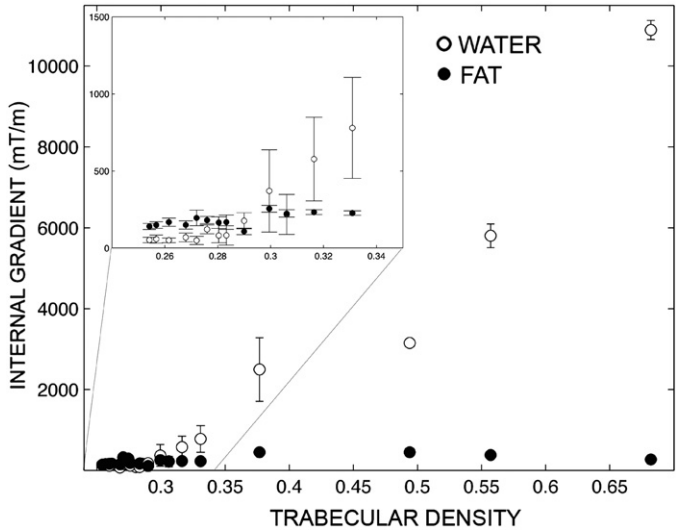

Figure 8. Water G_i behavior (empty circles) and fat G_i behavior (filled circles) as a function of trabecular density obtained as the ratio between the number of voxels belonging to the boundary perimeter (N_p) and the number of voxels of the whole area (N_a). The mean G_i values were calculated in a boundary region of three voxels wide. In the figure inset a zoom is displayed for TB densities ranging from 0.25 to 0.34.

The large SD associated with water G_i mean values is mainly due to differences in water content between the five samples. The strong variation of water ADC is likely due to the small differences in water–fat content percentages across samples. The larger the ADC SDs, the larger are the SDs of G_i. Conversely, the fat ADC changes less as a function of water–fat percentage variation.

Finally, T_2, ADC, G_i and T_2^{true} mean values and their SDs obtained from the entire slice area from each of the selected locations (averaging on the five samples) are reported in table 3. G_i and T_2^{true} were extracted from the fit by function (2), while T_2 and ADC represent values

Table 3. Results obtained from excised calf samples without discriminating between water and fat.

	($T_2 \pm$ SD) (ms)	(ADC $\pm$ SD) ($\times 10^{-10}$ m^2 s^{-1})	($G_i \pm$ SD) (mT m^{-1})	($T_2^{\text{true}} \pm$ SD) (ms)
LTD	22.6 ± 9.7	4.0 ± 0.7	263 ± 68	30.7 ± 3.3
ITD	22.0 ± 5.7	3.8 ± 1.2	411 ± 102	28.1 ± 2.9
HTD	8.7 ± 2.8	5.3 ± 1.6	675 ± 183	8.3 ± 1.2

Table 4. Calcaneus volunteer results.

Subject			Fat	($T_2^* \pm$ SD)	($T_2 \pm$ SD)	(ADC $\pm$ SD)	($G_i \pm$ SD)	($T_2^{\text{true}} \pm$ SD)
Sex	Age	Status	(%)	(ms)	(ms)	($\times 10^{-11}$ m^2 s^{-1})	(mT m^{-1})	(ms)
M	33	H	93	12.5 ± 3.1	34.6 ± 6.0	4.5 ± 0.9	894 ± 113	55.3 ± 7.1
F	24	H	87	9.8 ± 1.7	41.0 ± 3.7	4.3 ± 0.5	477 ± 40	41.3 ± 1.4
F	42	H	87	12.7 ± 2.3	35.3 ± 2.8	3.7 ± 0.7	415 ± 56	39.5 ± 1.9
F	52	H	88	9.5 ± 1.8	41.2 ± 3.2	5.0 ± 0.5	399 ± 44	40.6 ± 1.1
F	62	OPE	87	15.1 ± 2.3	42.0 ± 2.7	7.3 ± 0.5	311 ± 29	41.3 ± 0.9
F	62	OPO	90	21.1 ± 2.5	38.0 ± 2.5	6.6 ± 0.6	240 ± 47	47.0 ± 2.3

obtained by direct measures. Results reported in table 3 are from an additional analysis in which we did not discriminate between fat and water components. This means that both components contribute, with different modalities, to the total fitted signal. However, the acquisition parameters chosen for this experiment were intentionally optimized to focus on the water signal (for example, b values from 0 to 10 000 s mm^{-2} were chosen to detect the typical water ADC but not the fat ADC). This means that there is only a minimal weight of the fat component in the determined results reported in table 3.

T_2 and ADC values did not discriminate between LTD, ITD and HTD. Conversely, T_2^{true} was characterized by a decreasing trend when moving from LTD to HTD, while G_i showed different values in the three locations with different TB densities. In bone marrow, T_2 is mainly dependent on the relative proportion of fat and water protons (which are characterized by different transverse relaxation times), as well as from the TB density. The ADC depends on the interstitial spaces between bone and fat where water diffuses. G_i assumes a higher value for higher trabecular densities, as expected by water G_i values reported in table 3, which are due to differences in magnetic susceptibility at the bone–water interface.

Results reported in table 3 represent a preliminary test at high field to investigate the feasibility of including G_i measurements within clinical protocols (i.e. collection of T_2-weighted images and ADC maps). G_i would add useful information by discriminating between different TB densities.

3.2. In vivo results

Mean T_2^*, T_2, ADC, G_i and T_2^{true} with their corresponding SD values are summarized in table 4, together with the bone marrow fat content percentage extracted from the calcanei of six subjects. These findings indicate that T_2^*, T_2 and ADC do not discriminate between the

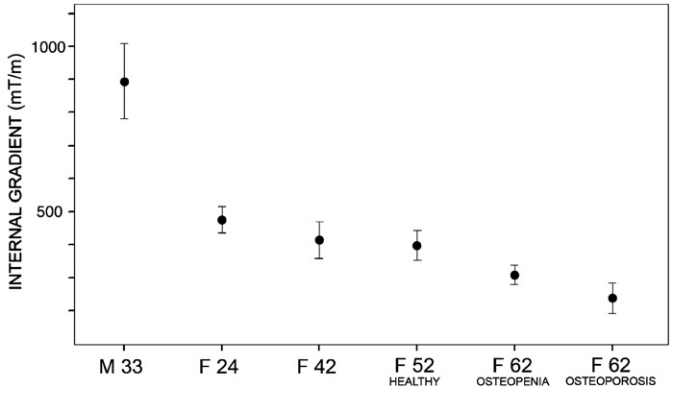

Figure 9. Clinical measures of G_i obtained from human calcanei as a function of individual 'supposed' TB densities. See the text for further details.

six different subjects presenting with different TB densities, while T_2^* discriminates between a healthy female of 52 years, and subjects with osteopenia and osteoporosis. Conversely, G_i discriminates between calcanei with different TB densities as shown in figure 9. Moreover, T_2^{true} values seem to be more associated with fat percentage than with TB densities.

According to the previous literature, the only male included in the current study showed a higher fat fraction when compared to females (Kugel *et al* 2001). The two youngest females (24 and 42 years old respectively) and the subject with osteopenia, showed a similar fat bone marrow percentage content with no evident differences related to aging. T_2^* was lower in the youngest female, characterized by a higher TB density when compared with the 42-year-old female. However, since T_2^* depends on both TB density and fat bone marrow concentrations, the male subject showed a higher T_2^*. Moreover, younger subjects were characterized by T_2^* values equal to those from a 52-year-old healthy subject characterized by a higher fat percentage value when compared to the 24-year-old female. Conversely, G_i values were remarkably different among subjects with different TB densities, independently from their bone marrow fat content.

The relationship between ADC *in vivo* and age/gender is less clear: a decreasing ADC for reduced BMD was reported in the vertebrae (Yeung *et al* 2004, Hatipoglu *et al* 2007), while other works reported a lack of correlation between diffusion indexes and BMD (Griffith *et al* 2006). The presence or absence of this relationship seems, therefore, to be related to different anatomical locations. Since the fat content in the calcaneus is higher than that observed in the spine (Liney *et al* 2007), the two sites are likely to be affected by BMD modifications in a different way. In the specific case of calcaneus spongy bone, restricted diffusion experienced by water confined between fat and bone could be hypothesized, as suggested by the ADC values reported in table 4, which are of the order of 10^{-11} m^2 s^{-1}. Moreover, a lower restricted diffusion due to increasing age or decreasing TB density could also be expected. However, it is not possible to conclude any general trend for all parameters listed in table 4 due to the small sample size.

Several studies reported an increase of T_2^* values for decreasing trabecular densities. However, the high inter-subject variability observed across studies is likely to be due to differences in water/fat ratios which affect T_2^* decay. Remarkably, higher values of T_2^* have been reported for fat as compared to the water component, either *in vitro* (Hussain *et al* 2005, O'Regan *et al* 2008) or *in vivo* (Weis *et al* 2008). Furthermore, several kinds of

fat molecules are present in bone tissue (Ren *et al* 2008), with relative concentration again varying across subjects. In table 4, T_2^* values of healthy subjects are very close to each other and overlap when considering their SDs. Moreover, the large T_2^* value reported for the male subject is more likely to be linked to a higher fat concentration rather than to a reduced TB density, which is not supported by any evidence from young healthy men. According to our experimental results, T_2^* turned out to be affected by the water/fat ratio, a parameter that shows a huge spread across different subjects. Some authors have suggested introducing corrections to account for variations in marrow composition (Wehrli *et al* 2000). However, to our knowledge, no-clinical studies involving these corrections have been published so far.

TB density is believed to be higher in male than in female subjects and to be lower in young than in elderly females. Moreover, TB density is lower in osteopenic subjects than in healthy subjects with the lowest values in females with osteoporosis. In our experiments, G_i has shown the ability to clearly discriminate between six subjects with different ages and different TB densities. Furthermore, G_i does not seem to suffer from the aforementioned limitation, which does not currently allow the clinical use of MR parameters on a single subject basis for diagnostic purposes. Clearly, our discussion about the potential clinical use of T_2^* and G_i parameters requires caution due to the small sample size recruited for the current study. In figure 9, G_i values presented are obtained from the central slice of the calcanei in six subjects, who presumably had different TB densities as expected in individuals with different sex, age and *T*-score values.

These results illustrate a smooth decrease of G_i values in the five females from the youngest to the oldest (linear correlation coefficient $r = 0.81$). Considering that age is a well-known factor affecting TB density, we can conclude that our preliminary data obtained *in vivo* demonstrate a progressive reduction of G_i across aging. With this perspective, we can speculate that G_i decreases proportionally with the physiological reduction of TB density. Future studies, including both large populations of healthy subjects and subjects with osteopenia and osteoporosis, are needed to clarify the potential diagnostic role of G_i. Moreover, it should be noted that our results, obtained *in vivo* by conventional T_2 and ADC measurement performed on a clinical scanner, fit well with those obtained *in vitro* (see figure 8).

The great potential of G_i as a novel marker for *in vivo* assessment of TB density relies on two different measurements, SE decay and ADC evaluation, which are needed to obtain G_i as a more specific parameter to reflect bone properties.

Since the fitting procedure involves the evaluation of the coefficient multiplying TE^3 in the second term of equation (2), the SD associated with G_i also depends on the uncertainty with which the ADC is known. From the statistical error propagation theory, the diffusion coefficient uncertainty affects the total variance with a term proportional to the square of the G_i times and the relative error associated with the ADC:

$$\frac{\sigma_{G_i}}{G_i} = \frac{\sigma_B}{B} + \frac{\sigma_D}{D}, \tag{3}$$

where $B = \frac{1}{12}\gamma^2 G_i^2 D$, σ_{G_i}, σ_B and σ_D are the SDs associated with G_i, B and ADC respectively. In a common experimental fit, B can be derived with a relative uncertainty of less than 10%. Also, an uncertainty of approximately 10% on the ADC measurement can be afforded using common clinical scanners. As a consequence, G_i can be estimated with a relative error that should not exceed 20%. From the perspective of a clinical application, this may guarantee the precision needed for G_i to discriminate among subjects characterized by different TB densities.

4. Conclusions

In this study, using high field microimaging to investigate spongy-bone samples, we demonstrate that water G_i is directly proportional to TB densities, while fat G_i does not provide specific information on bone's structural features. Moreover, we show that the concentration of water molecules at the bone–bone marrow interface is higher than that of fat molecules. It is further confirmed that measuring water MR parameters in spongy bone provides information on TB densities. To test G_i as a potential surrogate marker of TB density, we measured (using a clinical MR scanner) this parameter in the calcaneus of human subjects at different ages and with different DXA *T*-scores. In this experimental setting, we were able to detect only water G_i due to software and hardware limitations of clinical scanners. Data obtained *in vivo* demonstrated a progressive reduction of G_i across aging, thus suggesting that G_i decreases proportionally to the physiological reduction of TB density. Future studies, including both large populations of healthy subjects and patients with osteopenia and osteoporosis, are needed to clarify the potential diagnostic role of G_i in clinical protocols.

Acknowledgment

The authors thank Mr G Capuani for supplying the calf bone samples and for his information regarding the age and race of the calves.

References

Bousson V, Bergot C, Meunier A, Barbot F, Parlier-Cuau C, Laval-Jeantet A M and Laredo J-D 2000 CT of the middiaphyseal femur: cortical bone mineral density and relation to porosity *Radiology* **217** 179–87

Bousson V, Peyrin F, Bergot C, Hausard M, Sautet A and Laredo J-D 2004 Cortical bone in the human femoral neck: three-dimensional appearance and porosity using synchrotron radiation *J. Bone Miner. Res.* **19** 794–801

Capuani S, Rebuzzi M, Fasano F, Hagberg G E, Di Mario M, Vinicola V and Maraviglia B 2008 T_2^* relaxometry and ^{1}H-MRS at 3T applied to healthy and osteoporotic subjects: preliminary data supporting a new procedure to evaluate bone fracture risk *Proc. Intl. Soc. Mag. Reson. Med.* **16** 2534

Capuani S, Rossi C, Alesiani M and Maraviglia B 2005 Diffusion tensor imaging to study anisotropy in a particular porous system: the trabecular bone network *Solid State Nucl. Magn. Reson.* **28** 266–72

Carr H Y and Purcell E M 1954 Effects of diffusion on free precession in nuclear magnetic resonance experiments *Phys. Rev.* **94** 630–8

Chabanova E, Johnsen H E, Meldgaard Knudsen L, Larsen L, Logager V, Yingru S and Thomsen H S 2006 Magnetic resonace investigation of bone marrow following priming and stem cell mobilization *J. Magn. Reson. Imaging* **24** 1364–70

Chung H, Wehrli F W, Williams J L and Kugelmass S D 1993 Relationship between NMR transverse relaxation, trabecular bone architecture, and strength *Proc. Natl Acad. Sci. USA* **90** 10250–4

Griffith J F, Yeung D K W, Antonio G E, Wong S Y S, Wong T Y S, Kwok T C Y, Woo J and Leung P C 2006 Vertebral marrow fat content and diffusion and perfusion indexes in women with varying bone density: MR evaluation *Radiology* **241** 831–8

Hahn E L 1950 Spin echoes *Phys. Rev.* **80** 580–94

Hatipoglu H G, Selvi A, Ciliz D and Yuksel E 2007 Quantitative and diffusion MR imaging as a new method to assess osteoporosis *Am. J. Neuroradiol.* **28** 1934–7

Hussain H K, Chenevert T L, Londy F J, Gulani V, Swanson S D, McKenna B J, Appelman H D, Adusumilli S, Greenson J K and Conjeevaram H S 2005 Hepatic fat fraction: MR imaging for quantitative measurement and display—early experience *Radiology* **237** 1048–55

Hwang S N and Wehrli F W 1995 The calculation of the susceptibility-induced magnetic field from 3D NMR images with applications to trabecular bone *J. Magn. Reson.* **109** 126–45

Hwang S N and Wehrli F W 1999 Experimental evaluation of a surface charge method for computing the induced magnetic field in trabecular bone *J. Magn. Reson.* **139** 35–45

Kanis J A 2002 Osteoporosis III: diagnosis of osteoporosis and assessment of fracture risk *Lancet* **359** 1929–36

Kanis J A and Gluer C C 2000 An update on the diagnosis and assessment of osteoporosis with densitometry *Osteoporos. Int.* **11** 192–202

Kugel H, Jung C, Schulte O and Heindel W 2001 Age- and sex-specific differences in the ^{1}H-spectrum of vertebral bone marrow *J. Magn. Reson. Imaging* **13** 263–8

Kuntz J, Palmas P, Level V and Canet D 2008 Restricted diffusion and exchange of water in porous media: average structure determination and size distribution resolved from the effect of local field gradient on the proton NMR spectrum *J. Magn. Reson.* **191** 239–47

Lammentausta E, Silvast T S, Narvainen J, Jurvelin J S, Nieminen M T and Grohn O H J 2008 T_2, Carr–Purcell T_2 of fat and water as surrogate markers of trabecular bone structure *Phys. Med. Biol.* **53** 543–55

Liney G P, Bernard C P, Manton D J, Turnbill L W and Langton C M 2007 Age, gender and skeletal variation in bone marrow composition: a preliminary study at 3.0 Tesla *J. Magn. Reson. Imaging* **26** 787–93

Link T M, Majumdar S, Augat P, Lin J C, Newitt D, Lane N E and Genant H K 1998 Proximal femur: assessment for osteoporosis with T_2^* decay characteristics at MR imaging *Radiology* **209** 531–6

Majumdar S and Gore J C 1988 Studies of diffusion in random fields produced by variations in susceptibility *J. Magn. Reson.* **78** 41–55

Majumdar S, Thomasson D, Shimakawa A and Genant H K 1991 Quantitation of the susceptibility difference between trabecular bone and bone marrow: experimental studies *Magn. Reson. Med.* **22** 111–27

Mertens P, Machann J, Mueller-Bierl B, Steidle G, Bellemann M E and Schick F 2008 Magnetic field distribution in the presence of paramagnetic plates in magnetic resonance imaging: a combined numerical and experimental study *Med. Phys.* **35** 1777–84

Mosekilde L 2000 Age-related changes in bone mass, structure and strength—effects of loading *Z. Rheumatol.* **59** 1–9

Ong H H, Wright A C, Wehrli S L, Joses C E and Wehrli F W 2009 Is bone marrow diffusion too slow or too fast for susceptibility-based methods to assess trabecular bone architecture? *Proc. Intl. Soc. Magn. Reson. Med.* **17** 1941

O'Regan D P, Callaghan M F, Wylezinska-Arridge M, Fitzpatrick J, Naoumova R P, Hajnal J V and Schmitz S A 2008 Liver fat content and T_2^*: simultaneous measurement by using breath-hold multiecho MR imaging at 3.0 t feasibility *Radiology* **247** 550–7

Ren J, Dimitrov I, Sherry A D and Malloy C D 2008 Composition of adipose tissue and marrow fat in humans by ^{1}H NMR at 7 Tesla *J. Lipid Res.* **49** 2055–62

Sigmund E E, Cho H, Chen P, Byrnes S, Song Y–Q, Guo X E and Brown T R 2008 Diffusion-based MR methods for bone structure and evolution *Magn. Reson. Med.* **59** 28–39

Sigmund E E, Cho H and Song Y–Q 2009 High-resolution MRI of internal field diffusion-weighting in trabecular bone *NMR Biomed.* **22** 436–48

Szczepaniak L S, Dobbins R L, Stein D T and McGarry J D 2002 Bulk magnetic susceptibility effects on the assessment of intra-ad extramyocellular lipids *in vivo Magn. Reson. Med.* **47** 607–10

Thomsen J S, Ebbesen E N and Mosekilde L 2002 Age-related differences between thinning of horizontal and vertical trabeculae in human lumbar bone as assessed by a new computerized method *Bone* **31** 136–42

Watson A T and Chang C T P 1997 Characterizing porous media with NMR methods *Prog. Nucl. Magn. Reson. Spectrosc.* **31** 343–86

Wehrli F W, Ford J C, Attie M, Kressel H Y and Kaplan F S 1991 Trabecular structure: preliminary application of MR interferometry *Radiology* **179** 615–21

Wehrli F W, Ford J C and Haddad J G 1995 Osteoporosis: clinical assessment with quantitative MR imaging in diagnosis *Radiology* **196** 631–41

Wehrli F W, Hilaire L, Fernández-seara M, Gomberg B R, Kwon Song H, Zemel B, Loh L and Snyder P J 2002a Quantitative magnetic resonance imaging in the calcaneus and femur of women with varying degrees of osteopenia and vertebral deformity status *J. Bone Miner. Res.* **17** 2265–73

Wehrli F W, Hopkins J A, Hwang S N, Song H K, Snyder P J and Haddad J G 2000 Cross-sectional study of osteopenia with quantitative MR imaging and bone densitometry *Radiology* **217** 527–38

Wehrli F W, Kwon Song H, Saha P K and Wright A 2006 Quantitative MRI for the assessment of bone structure and function *NMR Biomed.* **19** 731–64

Wehrli F W, Saha P K, Gomberg B R, Song H, Snyder P J, Benito M, Wright A and Weening R 2002b Role of magnetic resonance for assessing structure and function of trabecular bone *Top. Magn. Reson. Imaging* **13** 335–56

Weis J, Johansson L, Ortiz-Nieto F and Ahlstrom H 2008 Assessment of lipids in skeletal muscle by high-resolution spectroscopic imaging using fat as the internal standard: comparison with water referenced spectroscopy *Magn. Reson. Med.* **59** 1259–65

WHO Scientific Group 2000 Prevention and management of osteoporosis *WHO Tech Report Series No 921*

Wilson R C and Hurlimann 2006 Relationship between susceptibility induced field inhomogeneities, restricted diffusion, and relaxation in sedimentary rocks *J. Magn. Reson.* **183** 1–12

Yeung D K W, Wong S Y S, Griffith J F and Lau E M C 2004 Bone marrow diffusion in osteoporosis: evaluation with quantitative MR diffusion imaging *J. Magn. Reson. Imaging* **19** 222–8